Eur. J. Mineral.
2003, **15**, 555–564

Dedicated to the memory
of Luciano Ungaretti

Sailaufite, (Ca, Na, □)$_2$Mn$_3$O$_2$(AsO$_4$)$_2$(CO$_3$)·3H$_2$O, a new mineral from Hartkoppe hill, Ober-Sailauf (Spessart mountains, Germany), and its relationship to mitridatite-group minerals and pararobertsite

MANFRED WILDNER[1]*, EKKEHART TILLMANNS[1], MICHAEL ANDRUT[1] and JOACHIM LORENZ[2]

[1]Institut für Mineralogie und Kristallographie der Universität Wien, Geozentrum, Althanstr. 14, A-1090 Wien, Austria
*Corresponding author, e-mail: manfred.wildner@univie.ac.at
[2]Graslitzer Str. 5, D-63791 Karlstein/Main, Germany

Abstract: Sailaufite, a new mineral with idealized composition CaNaMn$^{3+}{}_3$O$_2$(AsO$_4$)$_2$(CO$_3$)·3H$_2$O, has been found at the locality Hartkoppe hill near Ober-Sailauf (Spessart mountains, Germany), associated with hausmannite, arseniosiderite, kutnahorite, dolomite, quartz, calcite, and Mn-calcite. It occurs as strongly intergrown, dark red-brown to black tabular crystals, often forming mammillated coatings on calcite and arseniosiderite. Mohs' hardness is ~3.5, the cleavage is perfect parallel (001), the tenacity is brittle with an uneven to conchoidal fracture. Crystals are optically biaxial negative, at 616 nm n_α = 1.757(5), $\Delta_{\beta,\gamma}$ = 0.004(1), 2V = 32(3)°, n_β(calc) = 1.806, n_γ(calc) = 1.810. The strongest lines in the X-ray powder diffraction pattern are (d_{obs}, I, hkl): 8.807, 100, 001; 5.654, 27, 130; 5.544, 17, 200; 2.936; 75, 003; 2.885, 19, 331; 2.816, 20, 33$\bar{2}$; 2.772, 36, 400; 2.514, 20, 133; 2.202, 55, 004. UV-VIS-IR spectroscopic measurements confirm the presence of AsO_4 and CO_3 groups as well as the absence of transition metal ions other than Mn^{3+} in sailaufite. The crystal structure of a small untwinned crystal fragment could be solved by direct methods from X-ray CCD data [monoclinic, space group *Cm*, *a* = 11.253(1), *b* = 19.628(1), *c* = 8.932(1) Å, β = 100.05(1)°, Z = 6] and was refined on 8650 F_o^2 to *w*R2 = 0.079 and R1 = 0.045. The structure contains characteristic nonamer rings of edge-sharing $Mn^{3+}O_6$ octahedra forming compact pseudotrigonal [$Mn^{3+}{}_9O_6(AsO_4)_6(CO_3)_3]^{9-}$ sheets which are linked by layers composed of (Ca,Na,□)$O_5(H_2O)_2$ polyhedra and isolated water molecules. The octahedral nonamer rings correspond to those occuring in the Fe^{3+}-phosphate mitridatite and bear strong similarities to the arrangement of Z-shaped octahedral chains in the Mn^{3+}-phosphate pararobertsite.

Key-words: sailaufite, new mineral, crystal structure, arsenate, carbonate.

Introduction

Sailaufite, (Ca,Na,□)$_2$Mn$_3$O$_2$(AsO$_4$)$_2$(CO$_3$)·3H$_2$O, is a new mineral discovered at the locality Hartkoppe hill near Ober-Sailauf in the Spessart mountains, Germany. It was first suggested to be the Mn^{3+} analogon of arseniosiderite (Lorenz, 1991) and hence to belong to the mitridatite mineral group. However, a detailed structure investigation was hampered for many years due to severe intergrowth, twinning and stacking faults of crystals of suitable size. Now, it was possible to solve the crystal structure from X-ray CCD data obtained on a small untwinned crystal fragment, and to establish the structural relationships to mitridatite group minerals and to pararobertsite.

The mineral and mineral name have been approved by the IMA Commision on New Minerals and Mineral Names (no. 2000-005) prior to publication. Type material is deposited in the collection of the Institut für Mineralogie und Kristallographie der Universität Wien, Vienna, Austria.

Occurrence

The new mineral sailaufite was found for the first time in veins of manganese ore, exposed in the rhyolite body at Hartkoppe hill, north of Ober-Sailauf, Spessart mountains, NW-Bavaria, Germany. Here, it occurs as a very rare phase especially in carbonate-rich and braunite-depleted parts of the manganese ore veins, predominantly associated with hausmannite, arseniosiderite, kutnahorite, dolomite, quartz, calcite, and Mn-calcite. Newer findings of sailaufite in the lower parts of the Hartkoppe rhyolite quarry are in addition associated with rhodochrosite, brandtite, tilasite, and dolomite. A detailed description of the locality at Hartkoppe hill is given by Lorenz (1991), who also mentioned the new mineral as Mn-analogue of arseniosiderite. The mineral was formed in the last stages of low hydrothermal processes, which lead to the formation of manganese ore veins in the rhyolite body at Hartkoppe hill.

In the meantime, sailaufite was reported also from the Starlera Mn-deposit in the Eastern Alps of Switzerland (Brugger *et al.*, 2002). Here it occurs with manganlothar-

DOI: 10.1127/0935-1221/2003/0015-0555
0935-1221/03/0015-0555 $ 4.50

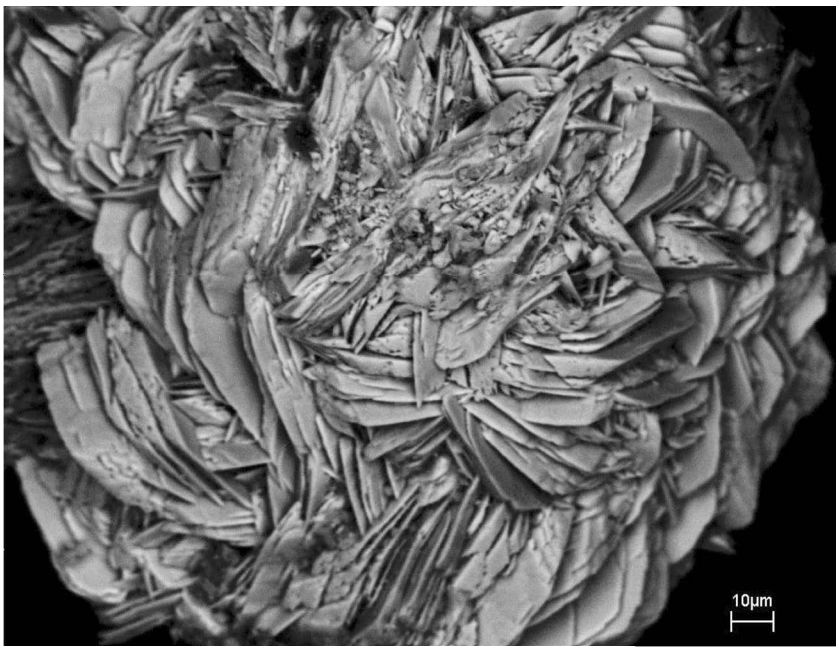

Fig. 1. SEM image of a typical crystal aggregate of sailaufite.

meyerite, tilasite, and calcite in discordant veinlets within massive braunite ore.

Appearance and physical properties

Sailaufite usually occurs as strongly intergrown tabular crystals, often forming mammillated coatings on calcite and arseniosiderite. Crystal aggregates are mostly <0.5 mm in size, and parts of single crystals are extracted by crushing the mineral aggregates. However, crystal fragments free of twinning or stacking faults are only rarely obtained and very small (<100 µm, mostly <50 µm.). Fig. 1 shows a SEM picture of a typical crystal aggregate. The macroscopic colour of sailaufite is dark red-brown to black with a brown streak and vitreous lustre. No fluorescence is observed with UV-light. Mohs' hardness is about 3.5, the cleavage is perfect parallel (001), the tenacity is brittle with an uneven to conchoidal fracture. Sailaufite crystals are slowly soluble in hydrochloric acid.

Sailaufite is optically biaxial negative. At a wavelength of 616 nm – the minimum of absorption in the visible range – n_α is 1.757(5). n_β and n_γ are > 1.8, but could not be determined precisely due to the strong VIS-absorption combined with the dark colour of the available immersion liquids. However, it was possible to measure $\Delta_{\beta,\gamma} = 0.004(1)$ as well as 2V = 32(3)°, and hence n_β and n_γ are calculated to be 1.806 and 1.810, respectively. The Gladstone-Dale relationship for the idealized formula yields <n> = 1.789, in perfect agreement with the measured data. The compatibility index $(1 - K_P/K_C) = -0.003$ is rated as superior. The orientation of the indicatrix axes is X ~c*, Y = b, Z ~a. The measured and calculated optical data are in very good agreement with the analysis of interferences of thin plane-parallel (001)-plates in the range 580–2400 nm (see section on spectroscopic investigations).

Chemical composition

An electron microprobe (EMP) analysis of sailaufite was obtained on a polished and carbon coated part of the same mineral grain, on which the structure analysis (see below) was done. The EMP analysis was performed on a Cameca SX100 with 15 kV operating voltage and 20 nA beam current using albite (Na_2O), CoAsS (As_2O_5), Mn (Mn_2O_3), and SI-8 (CaO) as standards. Due to the small grain size, only one meaningful analysis could be obtained. Furthermore, the mineral is unstable if exposed to the electron beam: loss of water and sodium migration were observed during the EMP measurement. Therefore the microprobe results are assumed to be subject to relatively large errors. The analysis yielded 1.76 wt.% Na_2O, 11.80 wt.% CaO, 38.20 wt.% Mn_2O_3, and 34.92 wt.% As_2O_5, giving a sum of 86.68 wt.%, the corresponding empirical formula of sailaufite based on 16 oxygen, one carbon, and six hydrogen atoms is $(Ca_{1.35}Na_{0.42}\square_x)Mn_{2.84}As_{2.13}O_{10}(CO_3)\cdot 3H_2O$, the idealized formula is $CaNaMn_3O_2(AsO_4)_2(CO_3)\cdot 3H_2O$. The presence of CO_3 groups and H_2O was confirmed by IR absorption and Raman spectroscopic measurements and by the single crystal structure refinement as outlined below.

Additional EMP analyses on other samples of this mineral are in principle agreement with the empirical formula quoted above, but show rather large variations, most probably due to chemical and structural inhomogenities (like severe stacking faults, *etc.*).

X-ray crystallography and crystal structure investigation

The powder diffraction data of sailaufite, listed in Table 1, were measured on a Philips X'Pert diffractometer with sample spinner using graphite monochromatized CuK_α radia-

Table 1. X-ray powder diffraction data for sailaufite.

I/I_o	d_{obs} (Å)	d_{calc} (Å)	h	k	l
100	8.7856	8.8070	0	0	1
27	5.6524	5.6538	1	3	0
17	5.5452	5.5441	2	0	0
14	4.9651	4.9664	1	3	–1
10	4.5718	4.5734	1	3	1
8	4.3968	4.4035	0	0	2
7	3.7898	3.7913	2	0	–2
5	3.6312	3.6373	1	3	–2
9	3.2883	3.2862	0	6	0
8	3.2190	3.2216	3	3	0
8	3.1891	3.1888	3	3	–1
4	3.0812	3.0788	0	6	1
75	2.9342	2.9357	0	0	3
19	2.8847	2.8850	3	3	1
20	2.8169	2.8158	3	3	–2
36	2.7702	2.7721	4	0	0
8	2.7110	2.7075	1	3	–3
15	2.6253	2.6235	2	6	1
7	2.5577	2.5596	4	0	–2
20	2.5144	2.5140	1	3	3
8	2.4871	2.4899	3	5	1
5	2.3565	2.3591	3	3	–3
3	2.2885	2.2867	2	6	2
3	2.2242	2.2219	4	0	–3
55	2.2016	2.2018	0	0	4
5	2.1490	2.1492	1	9	0
9	2.1289	2.1267	4	6	–1
7	2.1013	2.1013	5	3	0
4	2.0203	2.0199	3	3	3
3	1.9650	1.9648	3	3	–4
6	1.9486	1.9500	2	6	3
3	1.8966	1.8957	4	0	–4
4	1.8083	1.8097	3	9	1
7	1.7909	1.7922	3	9	–2
4	1.7480	1.7474	6	0	1
2	1.7256	1.7266	1	3	–5
4	1.7056	1.7064	6	0	–3
3	1.6991	1.6995	3	3	4
6	1.6659	1.6655	2	6	4
6	1.6574	1.6571	3	3	–5
9	1.6394	1.6401	1	3	5
16	1.6301	1.6297	6	6	–1
3	1.6131	1.6128	3	11	0
7	1.5925	1.5920	4	0	4
16	1.5600	1.5596	2	6	–5
1	1.4837	1.4835	4	8	3
5	1.4679	1.4678	0	0	6
4	1.4540	1.4537	3	3	5
6	1.4342	1.4338	0	12	3
3	1.4184	1.4182	2	12	–3
5	1.4073	1.4079	6	6	–4
5	1.3910	1.3905	1	3	6
3	1.3816	1.3813	7	3	2
2	1.3509	1.3509	1	13	–3
2	1.3279	1.3282	6	6	3
2	1.3168	1.3168	0	12	4
2	1.2926	1.2924	6	6	–5
1	1.2771	1.2768	2	0	–7
1	1.2640	1.2638	6	0	–6
2	1.2576	1.2581	0	0	7
2	1.2293	1.2293	4	14	1
3	1.2110	1.2111	3	15	–2
5	1.1775	1.1774	0	10	6
2	1.1697	1.1696	5	3	–7

Table 2. Crystal data and data collection details for sailaufite.

crystal size (μm)	75×40×15
crystal system	monoclinic
space group	*Cm* (No. 8)
a (Å)	11.253(1)
b (Å)	19.628(1)
c (Å)	8.932(1)
β (°)	100.05(1)
V (Å^3)	1942.6
Z	6
μ (cm^{-1})	85.3
D_{calc} (g cm^{-3})	3.356
$2\theta_{max}$	70
exposure time (s) / frame	2×180
CCD frames processed	456
frame scale factors$_{min\ /\ max}$	0.72/1.07
extinction coefficient	0.00048(4)
total number of intensity data	62751
number of reflections	39927
reflections for unit cell	19165
number of hkl's	18390
number of hkl's < 70° 2θ	16351
unique hkl's	8650
$F_o > 4\sigma(F_o)$	6830
R_i (%)	5.87
variables	385
*w*R2 [for all F_o^2] (%)	7.90
R1 [for $F_o > 4\ \sigma(F_o)$] (%)	4.48
R1 [for all F_o] (%)	6.70
goodness of fit	1.023
$\Delta\varrho_{max\ /\ min}$ (e$^-$Å^{-3})	1.43/–1.58

weighting scheme : $w = 1/[\sigma^2(F_o^2) + (0.0266P)^2]$;
$P = \{[\max \text{ of } (0 \text{ or } F_o^2)] + 2F_c^2\} / 3$

tion and Si as internal standard. The lattice parameters obtained by least-squares treatment of the powder data are a = 11.267(2) Å, b = 19.717(3) Å, c = 8.949(1) Å, β = 100.22(1)° *i.e.* slightly but significantly different from the results of the single crystal refinement given in Table 2. This is attributed to compositional variations of different samples of the mineral.

The crystal structure of sailaufite could be investigated using a small untwinned crystal fragment. X-ray diffraction intensities and lattice parameters were measured at room temperature on a Nonius Kappa CCD diffractometer with graphite monochromatized Mo*K*α radiation. In order to fill the complete Ewald sphere up to $2\theta = 70°$, several sets of φ- and ω-scans with 2° rotation per CCD-frame were performed at a crystal to detector distance of 28 mm. The extraction and correction of the intensity data, including a pseudo-absorption correction by frame scaling and the refinement of lattice parameters, were performed with the program DENZO-SMN (Nonius, 1998). The structure was solved in space group *Cm* by direct methods (SHELXS-97, Sheldrick 1997) and subsequent Fourier- and difference Fourier syntheses. The refinement on F^2 was done with the program SHELXL-97 (Sheldrick, 1997). In agreement with the chemical analysis, the refinement showed that three (sites A1-A3) out of four alkaline (earth) positions are not fully occupied with calcium, but also accomodate sodium

Table 3. Atomic coordinates and displacement parameters (Å^2) in sailaufite. The ADP are defined as $exp(-2\pi^2\Sigma_i\Sigma_j U_{ij}h_ih_j\boldsymbol{a}_i^*\boldsymbol{a}_j^*)$, the U_{eq} as $^1/_3\ \Sigma_i\Sigma_j U_{ij}\,\boldsymbol{a}_i^*\boldsymbol{a}_j^*\boldsymbol{a}_i\boldsymbol{a}_j$ (Fischer & Tillmanns, 1988).

atom	x	y	z	$U_{iso/eqv}$	U_{11}	U_{22}	U_{33}	U_{23}	U_{13}	U_{12}
As1	0.83715(7)	0	0.53900(9)	0.00691(16)	0.0072(3)	0.0066(3)	0.0070(4)	0	0.0013(3)	0
As2	0.42147(7)	0	0.97103(10)	0.00821(16)	0.0085(3)	0.0087(3)	0.0077(4)	0	0.0023(3)	0
As3	0.30697(5)	0.15817(3)	0.53815(6)	0.00754(12)	0.0076(2)	0.0075(2)	0.0075(3)	0.00011(18)	0.0014(2)	–0.00030(15)
As4	0.89143(5)	0.17537(3)	0.96652(6)	0.00767(12)	0.0080(2)	0.0078(2)	0.0073(3)	0.00029(19)	0.0017(2)	0.00072(16)
Mn1	0.62816(9)	0	0.25465(14)	0.0061(2)	0.0044(5)	0.0078(4)	0.0063(6)	0	0.0015(4)	0
Mn2	0.10012(9)	0.16687(5)	0.24963(13)	0.00534(14)	0.0028(3)	0.0066(3)	0.0066(4)	0.00016(15)	0.0006(3)	0.00013(16)
Mn3	0.34947(7)	0.24145(4)	0.25145(9)	0.00522(15)	0.0050(3)	0.0046(3)	0.0059(4)	–0.0004(3)	0.0006(3)	–0.0018(2)
Mn4	0.86236(9)	0.08735(4)	0.24994(13)	0.00550(12)	0.0061(2)	0.0036(2)	0.0067(3)	0.0006(2)	0.0009(2)	–0.0012(2)
Mn5	0.36306(9)	0.07965(4)	1.25199(13)	0.00544(12)	0.0062(3)	0.0044(2)	0.0059(3)	–0.0004(2)	0.0014(2)	0.0014(2)
A1*	0.21795(19)	0.15628(9)	0.9255(3)	0.0142(5)	0.0128(9)	0.0189(8)	0.0109(11)	–0.0005(7)	0.0019(8)	–0.0007(6)
A2*	0.7553(3)	0	0.9254(4)	0.0130(7)	0.0186(15)	0.0120(12)	0.0082(16)	0	0.0019(12)	0
A3*	0.97944(11)	0.17535(5)	0.58638(17)	0.0115(2)	0.0121(5)	0.0105(4)	0.0117(6)	–0.0002(4)	0.0016(4)	0.0008(3)
Ca4	0.51193(14)	0	0.5864(2)	0.0112(3)	0.0109(7)	0.0128(6)	0.0102(8)	0	0.0029(6)	0
C1	0.1038(7)	0	0.2328(11)	0.0115(17)	0.005(3)	0.002(3)	0.030(5)	0	0.007(3)	0
C2	0.1107(7)	0.3336(3)	0.2603(9)	0.0067(8)	0.0073(17)	0.0117(17)	0.001(2)	–0.0007(10)	–0.0005(15)	–0.0003(11)
Ow1	0.1924(5)	0	0.6078(8)	0.0174(12)	0.014(3)	0.020(3)	0.018(4)	0	0.004(2)	0
Ow2	0.5288(4)	0.16292(16)	0.9100(6)	0.0235(10)	0.021(2)	0.025(2)	0.025(3)	0.0004(15)	0.007(2)	–0.0001(13)
O1	0.8747(5)	0	0.7249(7)	0.0111(11)	0.012(2)	0.015(2)	0.006(3)	0	0.000(2)	0
O2[#]	0.6877(5)	0	0.4770(7)	0.0100(11)	0.0015(19)	0.015(2)	0.015(3)	0	0.006(2)	0
O3	0.8939(4)	0.07107(17)	0.4685(5)	0.0090(8)	0.0101(16)	0.0101(14)	0.005(2)	0.0013(13)	–0.0026(14)	–0.0045(13)
O4	0.3573(4)	0.06936(17)	1.0371(5)	0.0085(7)	0.0115(17)	0.0075(14)	0.0064(19)	0.0014(13)	0.0006(14)	0.0035(12)
O5	0.4058(5)	0	0.7847(7)	0.0129(11)	0.015(3)	0.018(2)	0.005(3)	0	0.000(2)	0
O6	0.5710(5)	0	0.0409(7)	0.0093(11)	0.008(2)	0.012(2)	0.009(3)	0	0.005(2)	0
O7	0.3253(4)	0.15729(19)	0.7234(6)	0.0145(9)	0.0114(19)	0.0232(19)	0.009(2)	–0.0003(14)	0.0020(16)	0.0031(13)
O8	0.1561(3)	0.15711(19)	0.4657(5)	0.0097(8)	0.0043(17)	0.0139(16)	0.011(2)	0.0004(13)	0.0003(16)	–0.0033(11)
O9	0.3694(3)	0.22778(17)	0.4728(5)	0.0080(7)	0.0095(16)	0.0078(14)	0.0072(19)	0.0027(13)	0.0028(14)	–0.0022(12)
O10	0.3730(4)	0.08885(17)	0.4715(5)	0.0098(8)	0.0118(17)	0.0090(15)	0.008(2)	–0.0012(14)	0.0013(14)	0.0071(13)
O11	0.8322(3)	0.10483(18)	1.0369(5)	0.0104(8)	0.0147(18)	0.0086(14)	0.008(2)	0.0012(14)	0.0019(15)	–0.0055(13)
O12	1.0419(4)	0.17590(19)	1.0343(5)	0.0097(8)	0.0080(16)	0.0176(17)	0.002(2)	–0.0009(13)	–0.0024(14)	–0.0001(13)
O13	0.8302(4)	0.24504(18)	1.0379(5)	0.0107(8)	0.0135(18)	0.0109(15)	0.009(2)	–0.0002(14)	0.0045(15)	0.0032(13)
O14	0.8575(4)	0.17604(17)	0.7796(5)	0.0124(8)	0.0155(19)	0.0158(16)	0.006(2)	–0.0004(12)	0.0025(16)	0.0001(13)
O15	0.2598(3)	0.15674(16)	0.2132(5)	0.0047(7)	0.0026(14)	0.0058(13)	0.005(2)	0.0007(11)	–0.0011(13)	0.0001(10)
O16	0.4378(4)	0.32466(16)	0.2933(5)	0.0069(8)	0.0068(15)	0.0041(13)	0.011(2)	–0.0007(12)	0.0041(15)	0.0008(10)
O17	0.7896(4)	0	0.2126(7)	0.0057(10)	0.0047(19)	0.0051(19)	0.006(3)	0	–0.0023(18)	0
O18	0.4666(4)	0	1.2966(7)	0.0066(10)	0.005(2)	0.0050(18)	0.009(3)	0	0.0000(18)	0
O19	0.0491(3)	0.05692(16)	0.2336(5)	0.0103(8)	0.0056(15)	0.0071(15)	0.018(2)	–0.0001(14)	0.0028(15)	0.0016(12)
O20	0.1637(3)	0.27526(15)	0.2638(4)	0.0111(7)	0.0077(14)	0.0060(13)	0.019(2)	0.0015(13)	0.0006(13)	–0.0002(11)
O21	0.2220(4)	0	0.2507(7)	0.0101(11)	0.001(2)	0.008(2)	0.021(3)	0	0.003(2)	0
O22	–0.0047(3)	0.33592(12)	0.2489(5)	0.0120(9)	0.0042(16)	0.0075(15)	0.024(3)	0.0019(10)	0.0009(16)	0.0018(9)
O23	0.1723(3)	0.38808(15)	0.2653(4)	0.0128(7)	0.0094(15)	0.0063(14)	0.023(2)	–0.0023(13)	0.0042(14)	0.0000(12)
O24	0.0756(3)	0.0883(2)	0.7598(5)	0.0156(9)	0.016(2)	0.016(2)	0.013(2)	–0.0012(15)	–0.0001(17)	0.0003(14)
O25	0.6392(4)	0.08056(19)	0.7386(6)	0.0208(9)	0.0166(19)	0.0205(18)	0.025(3)	–0.0080(17)	0.0033(18)	–0.0015(15)
O26	1.1209(3)	0.2469(2)	0.7418(6)	0.0207(10)	0.014(2)	0.0167(17)	0.031(3)	–0.0112(16)	0.0037(18)	–0.0074(15)
H11[§]	0.159(5)	0.0377(10)	0.574(9)	0.057(8)[+]						
H12[§]	0.265(6)	0	0.658(12)	0.057(8)						
H21	0.474(5)	0.133(3)	0.852(7)	0.057(8)						
H22	0.512(6)	0.170(3)	0.996(5)	0.057(8)						
H241	0.096(5)	0.038(2)	0.727(7)	0.057(8)						
H242	–0.007(4)	0.070(3)	0.755(7)	0.057(8)						
H251	0.700(5)	0.107(3)	0.703(7)	0.057(8)						
H252	0.607(6)	0.102(3)	0.806(7)	0.057(8)						
H261	1.104(6)	0.273(3)	0.817(6)	0.057(8)						
H262	1.175(5)	0.262(3)	0.696(6)	0.057(8)						

* refined A-site occupancies (restrain $X_{Ca}+X_{Na}=1$): A1: 0.207(4)Ca+0.793(4)Na, A2: 0.046(4)Ca+0.954(4)Na, A3: 0.987(4)Ca+0.013(4)Na

[§] fixed H11 and H12 occupancy: 2/3

[+] common U_{iso} refined for all H-atoms

[#] ADP(O2) non positive definite

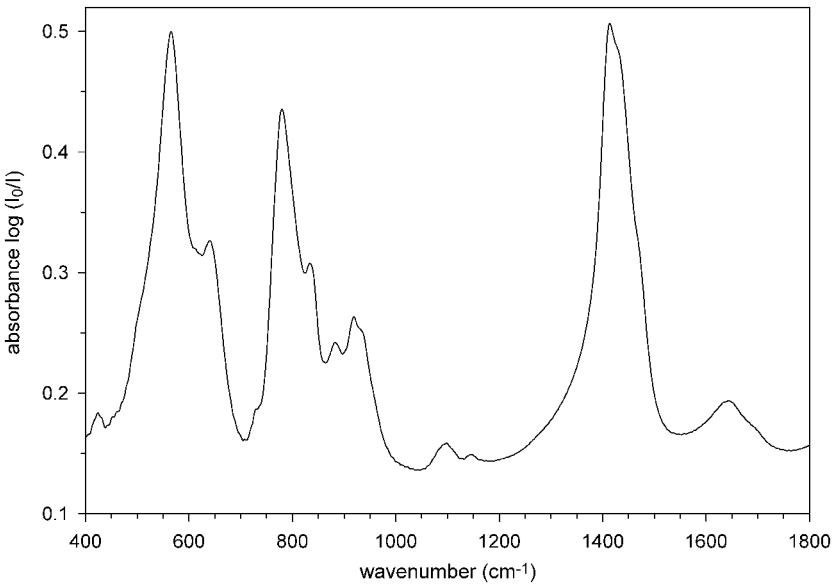

Fig. 2. IR absorption powder spectrum of sailaufite in the spectral region between 400 and 1800 cm^{-1}.

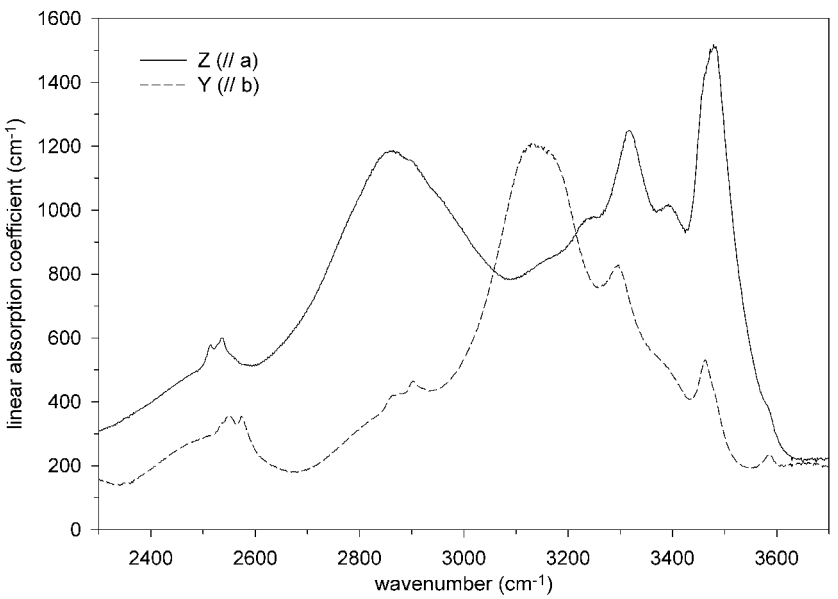

Fig. 3. Polarized IR absorption spectra in the OH stretching vibrational region obtained on a (001) platelet of sailaufite.

atoms and/or vacancies. In the final stages of the anisotropic refinement, hydrogen positions could be located in difference Fourier maps and refined applying soft restraints and a common isotropic displacement parameter. The Ow1 water molecule comprises three possible hydrogen positions (H12, and two H11 equivalent by the mirror plane). They were each fixed at an occupancy of 2/3 in the final refinement. Crystal data as well as further details of the data collection and structure refinement are given in Table 2, Table 3 lists final atomic coordinates and displacement parameters.

Spectroscopic investigations

Polarized absorption spectra of a 7.5 µm thin (001) cleavage-platelet of sailaufite were measured at room temperature in the IR-NIR-VIS spectral range between 600 cm^{-1} and 20500 cm^{-1} on a Bruker IFS 66v/S FTIR-Spectrometer using the attached mirror optics microscope IR-scopeII. Despite the small sample thickness, several vibrational modes <1500 cm^{-1} exceeded the sensitivity limits of the instrument. Therefore, additional IR-powder spectra (KBr pellets) were recorded between 400 and 3800 cm^{-1} in the vacuum sample chamber. The spectral bandwidth was 10 cm^{-1} in the NIR/VIS range and 2 cm^{-1} in the infrared range, the local resolution of the single crystal measurements was 40 µm in both spectral regions. Appropriate combinations of light sources (globar, tungsten lamp), beam splitters (KBr, quartz), detectors (MCT, Si-diode, Ge-diode, GaP-diode) and polarizers (wire grid polarizer KRS-5, calcite Glan-prism) were used. Raman spectra in the range 200 to 1800 cm^{-1} were obtained on a Renishaw RM 1000 research-grade Raman spectrometer (two notch filter system, 1200

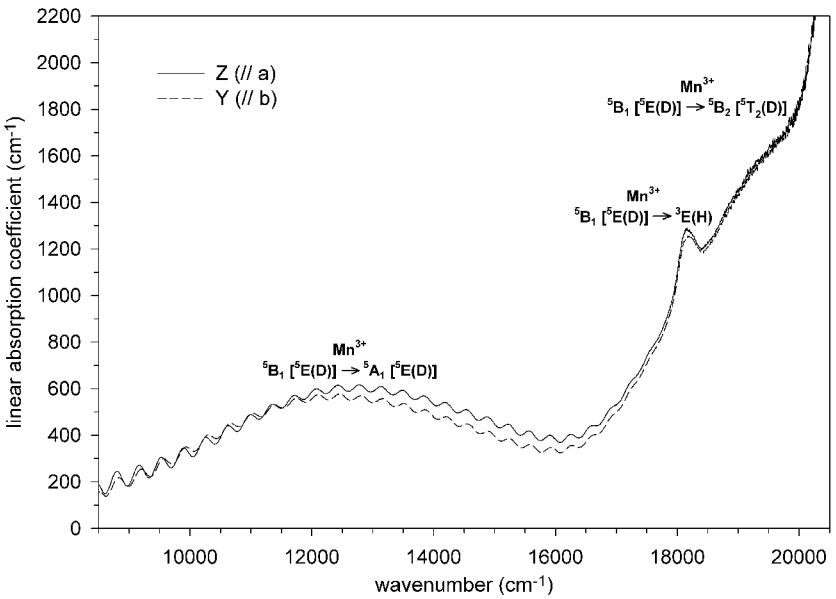

Fig. 4. Polarized NIR-VIS electronic absorption spectra obtained on a (001) platelet of sailaufite and assignment of Mn^{3+} d-d transitions. Observed interferences were used to confirm the values of n_β and n_γ calculated from the Gladstone-Dale relationship.

grooves/mm grating, Peltier-cooled CCD detector) equipped with a Leica DMLM series microscope. A Leica 100x objective was used (numerical aperture = 0.95) resulting in a measuring spot size of approximately 2 μm. Spectra were excited with the 633 nm line of a He-Ne laser. Fig. 2 shows the IR-powder spectra between 400-1800 cm^{-1}, Fig. 3 the Y- and Z-polarized IR-spectra between 2300-3700 cm^{-1}, and Fig. 4 the respective polarized spectra in the NIR-VIS region from 8500-20500 cm^{-1}. The NIR region between 3600 and 8000 cm^{-1} shows no absorptions in Y- and Z-polarization. Here and in the visible spectral range (Fig. 4), observed interferences were used to confirm the calculated values of n_β and n_γ, which could not be measured directly using the immersion method (see section on physical properties above).

The IR powder (Fig. 2) and single crystal Raman spectra clearly confirm the presence of both, CO_3 and AsO_4 groups in the structure of sailaufite. Bands or band components observed in the IR- or Raman spectra around 730, 880, 1120, and 1420 cm^{-1} can be assigned to the ν_4, ν_2, ν_1, and ν_3 vibrational modes, respectively, of the two different CO_3 groups. Bands caused due to different AsO_4 groups are located around 350-450 (ν_4 and ν_2) and 780-940 cm^{-1} (ν_3 and ν_1). Intense spectral features in the region between 500-680 cm^{-1} are attributed to stretching modes involving Mn–O bonds. H_2O bending modes are found at 1640 cm^{-1} with a shoulder at 1695 cm^{-1}.

Several clearly polarized absorption bands occur in the region of the H_2O streching vibrational modes (Fig. 3). The most prominent spectral features are located at about 2860, 3230, 3320, 3395, and 3480 cm^{-1} in Z-polarization, and at about 3130, 3295, 3460, and 3585 cm^{-1} in Y-polarization. The fine structure at 2515-2575 cm^{-1} and around 2900 cm^{-1} can be attributed to the $\nu_1 + \nu_3$ combination mode and to the first overtone of ν_3, respectively, of the carbonate groups.

The absorption features in the NIR and visible spectral regions (Fig. 4) are assigned to d-d transitions of Mn^{3+} in Jahn-Teller distorted octahedral coordination. In agreement with the pseudotrigonal topology of the octahedral nonamer rings (see below) oriented parallel (001), the optical Y- and Z-spectra are practically not polarized at all. The very broad band at ~12500 cm^{-1} represents the $^5A_1$ level of the $^5E(D)$ ground state in O_h symmetry, which is split up by the strong pseudotetragonal Jahn-Teller distortion of the octahedra into $^5A_1$ and the new ground state $^5B_1$. Within the low energy wing of the CT absorption edge, another spin-allowed transition, $^5B_1 \rightarrow {}^5B_2(^5T_2)$ is observed at ~19000 cm^{-1}, as well as a sharp spin-forbidden transition to a split level of the field independent ^3E level, arising from the ^3H free ion term. The optical absorption spectra give no indications for significant amounts of manganese in other oxidation states or for the presence of transition metal ions other than Mn^{3+}.

Description and discussion of the structure

Important interatomic bond lengths and angles in sailaufite are listed in Table 4, sections of the crystal structure in projections along [001] are shown in Fig. 5 and 6. The main structural building blocks are compact pseudotrigonal $[Mn^{3+}{}_9O_6(AsO_4)_6(CO_3)_3]^{9-}$ sheets (Fig. 5) which are linked by layers built up from $(Ca,Na,\square)O_5(H_2O)_2$ polyhedra and free, *i.e.* only hydrogen bonded, water molecules (Fig. 6). The $[Mn^{3+}{}_9O_6(AsO_4)_6(CO_3)_3]^{9-}$ sheets are composed of five crystallographically distinct $Mn^{3+}O_6$ octahedra forming edge-sharing nonamer rings, two types of CO_3 groups occupying the centres of these rings as well as the voids between each three neighbouring rings, and four different AsO_4 tetrahedra each sharing three corners with remaining octahedral vertices.

In accordance with the d^4 electron configuration of Mn^{3+}, the MnO_6 octahedra are strongly Jahn-Teller distorted to elongated pseudotetragonal dipyramids. The bond length distortion of all five MnO_6 polyhedra is rather uniform, with overall mean bond lengths of 1.928 Å for the four short Mn–O bonds, and 2.232 Å for the two longer bonds. On the other

Table 4. Selected interatomic bond lengths (Å) and angles (°) in sailaufite.

C1–O19	2x	1.276(5)	O19–C1–O19		122.2(7)
C1–O21		1.311(9)	O19–C1–O21	2x	118.6(4)
<C1–O>		1.288			
C2–O20		1.288(7)	O20–C2–O22		119.4(5)
C2–O22		1.285(8)	O20–C2–O23		120.0(6)
C2–O23		1.271(7)	O22–C2–O23		120.7(5)
<C2–O>		1.281			
As1–O1		1.640(6)	O1–As1–O2		113.6(3)
As1–O2		1.676(5)	O1–As1–O3	2x	109.1(2)
As1–O3	2x	1.700(4)	O2–As1–O3	2x	107.3(2)
<As1–O>		1.679	O3–As1–O3		110.3(3)
As2–O4	2x	1.695(4)	O4–As2–O4		106.9(3)
As2–O5		1.643(6)	O4–As2–O5	2x	112.1(2)
As2–O6		1.690(6)	O4–As2–O6	2x	109.2(2)
<As2–O>		1.681	O5–As2–O6		107.4(3)
As3–O7		1.631(5)	O7–As3–O8		109.0(2)
As3–O8		1.709(4)	O7–As3–O9		111.9(2)
As3–O9		1.687(3)	O7–As3–O10		111.1(2)
As3–O10		1.707(3)	O8–As3–O9		109.0(2)
<As3–O>		1.683	O8–As3–O10		108.8(2)
			O9–As3–O10		107.0(2)
As4–O11		1.703(4)	O11–As4–O12		107.7(2)
As4–O12		1.695(4)	O11–As4–O13		107.7(2)
As4–O13		1.704(4)	O11–As4–O14		110.1(2)
As4–O14		1.647(5)	O12–As4–O13		107.8(2)
<As4–O>		1.687	O12–As4–O14		113.7(2)
			O13–As4–O14		109.6(2)
Mn1–O2		1.982(7)	O2–Mn1–O17		91.7(2)
Mn1–O6		1.906(6)	O2–Mn1–O18		88.3(2)
Mn1–O17		1.918(5)	O2–Mn1–O23	2x	85.7(1)
Mn1–O18		1.919(5)	O6–Mn1–O17		88.2(2)
Mn1–O23	2x	2.251(3)	O6–Mn1–O18		91.7(2)
<Mn1–O>		2.038	O6–Mn1–O23	2x	94.3(1)
			O17–Mn1–O23	2x	78.4(1)
O2–Mn1–O6		180.0(2)	O18–Mn1–O23	2x	101.6(1)
O17–Mn1–O18		180.0(3)	σ_{oct}^2 = 56.7		
O23–Mn1–O23		154.9(2)			
Mn2–O8		1.932(5)	O8–Mn2–O15		90.5(2)
Mn2–O12		1.929(5)	O8–Mn2–O16		87.8(2)
Mn2–O15		1.892(4)	O8–Mn2–O19		90.2(2)
Mn2–O16		1.940(4)	O8–Mn2–O20		89.6(2)
Mn2–O19		2.231(3)	O12–Mn2–O15		90.3(2)
Mn2–O20		2.241(3)	O12–Mn2–O16		91.4(2)
<Mn2–O>		2.028	O12–Mn2–O19		89.2(2)
			O12–Mn2–O20		91.1(2)
O8–Mn2–O12		179.1(2)	O15–Mn2–O19		97.4(1)
O15–Mn2–O16		178.0(2)	O15–Mn2–O20		78.8(1)
O19–Mn2–O20		176.2(2)	O16–Mn2–O19		81.7(1)
			O16–Mn2–O20		102.1(1)
			σ_{oct}^2 = 36.8		
Mn3–O9		1.969(4)	O9–Mn3–O15		91.4(2)
Mn3–O13		1.900(5)	O9–Mn3–O16		87.5(2)
Mn3–O15		1.944(4)	O9–Mn3–O20		86.2(2)
Mn3–O16		1.915(3)	O9–Mn3–O22		87.8(2)
Mn3–O20		2.215(3)	O13–Mn3–O15		88.7(2)
Mn3–O22		2.239(3)	O13–Mn3–O16		92.4(2)
<Mn3–O>		2.030	O13–Mn3–O20		93.7(2)
			O13–Mn3–O22		92.3(2)
O9–Mn3–O13		179.8(2)	O15–Mn3–O20		78.5(1)
O15–Mn3–O16		178.9(2)	O15–Mn3–O22		77.1(1)
O20–Mn3–O22		154.7(1)	O16–Mn3–O20		101.4(1)
			O16–Mn3–O22		102.9(1)
			σ_{oct}^2 = 59.0		
Mn4–O3		1.949(5)	O3–Mn4–O16		87.1(2)
Mn4–O11		1.905(5)	O3–Mn4–O17		91.5(2)
Mn4–O16		1.934(3)	O3–Mn4–O19		90.7(2)
Mn4–O17		1.904(2)	O3–Mn4–O23		89.0(2)
Mn4–O19		2.214(3)	O11–Mn4–O16		92.0(2)
Mn4–O23		2.220(3)	O11–Mn4–O17		89.5(2)
<Mn4–O>		2.021	O11–Mn4–O19		89.3(2)
			O11–Mn4–O23		91.0(2)
O3–Mn4–O11		179.0(2)	O16–Mn4–O19		82.3(1)
O16–Mn4–O17		178.5(3)	O16–Mn4–O23		100.8(1)
O19–Mn4–O23		176.9(1)	O17–Mn4–O19		97.5(2)
			O17–Mn4–O23		79.5(2)
			σ_{oct}^2 = 32.8		
Mn5–O4		1.919(5)	O4–Mn5–O15		89.3(2)
Mn5–O10		1.952(5)	O4–Mn5–O18		92.0(2)
Mn5–O15		1.902(3)	O4–Mn5–O21		91.2(2)
Mn5–O18		1.949(3)	O4–Mn5–O22		88.4(2)
Mn5–O21		2.227(3)	O10–Mn5–O15		92.1(2)
Mn5–O22		2.231(3)	O10–Mn5–O18		86.7(2)
<Mn5–O>		2.030	O10–Mn5–O21		89.2(2)
			O10–Mn5–O22		91.3(2)
O4–Mn5–O10		178.5(2)	O15–Mn5–O21		98.4(2)
O15–Mn5–O18		178.4(3)	O15–Mn5–O22		78.1(1)
O21–Mn5–O22		176.5(2)	O18–Mn5–O21		80.7(2)
			O18–Mn5–O22		102.8(2)
			σ_{oct}^2 = 44.4		
A1–O4		2.412(4)	A3–O3		2.423(4)
A1–O7		2.341(5)	A3–O8		2.447(4)
A1–O12		2.386(4)	A3–O9		2.395(4)
A1–O13		2.432(5)	A3–O14		2.385(4)
A1–O15		2.530(5)	A3–O16		2.578(5)
A1–O24		2.390(5)	A3–O24		2.430(5)
A1–O26		2.534(5)	A3–O26		2.379(4)
<A1–O>		2.432	<A3–O>		2.434
A2–O1		2.419(6)	Ca4–O2		2.354(5)
A2–O6		2.472(6)	Ca4–O5		2.302(6)
A2–O11	2x	2.382(4)	Ca4–O10	2x	2.445(4)
A2–O17		2.527(7)	Ca4–O18		2.550(6)
A2–O25	2x	2.496(5)	Ca4–O25	2x	2.392(5)
<A2–O>		2.453	<Ca4–O>		2.412

hand, considering the bond angle distortion, two groups of MnO_6 octahedra can be distinguished, namely those sharing two *cis*-arranged edges with neighbouring octahedra, and those sharing two *trans*-arranged edges. The former (Mn1 and Mn3), representing the 'corners' of the nonamer rings, are characterized by one strongly bent octahedral axis (155°) and a generally stronger angle distortion, the latter (Mn2, Mn4, and Mn5) exhibit nearly straight octahedral axes and also weaker *cis*-angle distortions σ_{oct}^2. However, these smaller σ_{oct}^2 values can also be attributed predominantly to the octahedral edge sharing. Fig. 5 illustrates the

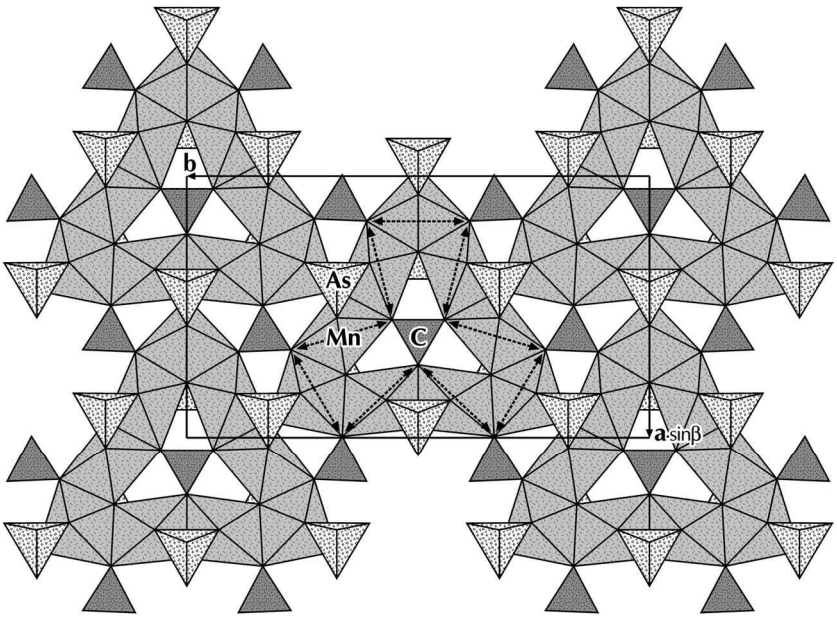

Fig. 5. Projection of the pseudotrigonal $[Mn^{3+}{}_9O_6(AsO_4)_6(CO_3)_3]^{9-}$ sheet in sailaufite along [001]. The dashed arrows indicate the Jahn-Teller elongation of the $Mn^{3+}O_6$ octahedra within the nonamer rings.

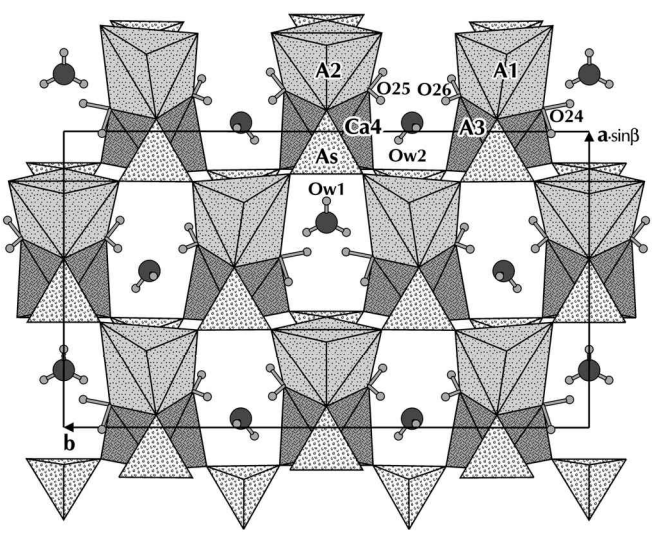

Fig. 6. Projection of the layer built up from $(Ca,Na,\square)O_5(H_2O)_2$ polyhedra, condensed to dimers, and isolated water molecules in sailaufite along [001]. The A1 and A2 sites are preferentially occupied by sodium, while A3 is practically fully and Ca4 is fully occupied by calcium. The water molecule Ow1 is disordered among three different orientations.

topological arrangement and shows that the elongated octahedral axes (marked by arrows) are located within the plane of the sheet, namely directed towards the common corners with CO_3 groups.

The geometries of the carbonate groups comply with crystal chemical experience. The C1 group occupies the centre of the octahedral nonamer rings and is slightly distorted with a mean C–O distance of 1.288 Å. The nearly regular C2 group, <C–O> = 1.281 Å, is located at the centres of six-membered octahedral rings, which are formed by each three adjacent nonamer rings.

Generally, the AsO_4 tetrahedra also comply closely with crystal chemical expectations. The overall mean distance <<As–O>> = 1.682 Å agrees with the value given by Baur (1981). The detailed geometries of the AsO_4 tetrahedra are influenced by their polyhedral linkages. Each AsO_4 group shares the O atoms of three long As–O bonds with each one Mn and one Ca/Na, while the remaining short As–O bond links only to one Ca/Na polyhedron. In particular, As1 and As3 each link three MnO_6 polyhedra within the same nonamer ring (on the back side of the octahedral sheet in Fig. 5), whereas As2 and As4 each link three MnO_6 polyhedra within two adjacent rings (on the top side in Fig. 5).

The layers consisting of four different $(Ca,Na,\square)O_5(H_2O)_2$ polyhedra and two water molecules (Fig. 6) link the octahedral-tetrahedral sheets along the c-axis. The A1 and A2 alkaline (earth) sites are preferentially occupied by sodium and subsidiary vacancies, while A3 is practically fully and Ca4 is fully occupied by calcium atoms. Each one sodium and one calcium polyhedron, namely A1 and A3 as well as A2 and Ca4, share their H_2O–H_2O edges forming $NaCaO_{10}(H_2O)_2$ dimers. In reverse analogy with the corner linkage between AsO_4 tetrahedra and MnO_6 octahedra, the polyhedra of A1 and A2 each share three egdes with a single nonamer ring, while A3 and Ca4 each share three edges with two adjacent nonamers. All A/CaO_7 polyhedra exhibit an irregular shape with mean values ranging between 2.412 Å and 2.453 Å. In accordance with the slightly different ionic radii of Ca^{2+} and Na^+ (Shannon 1976), these limiting values belong to the pure CaO_7 polyhedron (Ca4) and to the predominant NaO_7 polyhedron (A2), respectively.

The proposed hydrogen bonding system in sailaufite involving five different water molecules is summarized in Table 5. According to this scheme, the following O atoms act as acceptor for hydrogen bonds: the common corners of AsO_4 and Na/CaO_7 polyhedra (O1, O5, O7, O14), the free water molecules (Ow1, Ow2) themselves, one oxygen (O8) linking As, Mn, and Na/Ca, and finally a common corner

Table 5. The hydrogen bonding system (Å, °) in sailaufite.

D–H ···A	D–H	D···A	D–H···A
Ow1 –H11···O8	0.86(3)	3.333(5)	155(7)
–H12···O5	0.86(4)	2.633(9)	172(9)
Ow2 –H21···O7	0.94(4)	2.590(7)	127(5)
–H22···O22	0.83(4)	3.115(7)	164(6)
O24 –H241···Ow1	1.06(4)	2.682(6)	137(4)
–H242···O1	0.99(4)	2.822(6)	154(5)
O25 –H251···O14	0.95(4)	3.060(5)	143(5)
–H252···Ow2	0.86(4)	2.677(6)	166(7)
O26 –H261···Ow2	0.90(4)	2.647(6)	159(7)
–H262···O14	0.85(4)	3.030(5)	133(5)

(O22) between two Mn and a carbonate group. However, this hydrogen bonding scheme complies only roughly with the observed IR-polarization behaviour (Fig. 3) or with the respective band positions predicted according to D···A–frequency correlations (*e.g.* Libowitzky, 1999). This indicates that especially the free water molecules Ow1 and Ow2 might be directionally as well as positionally disordered, and that the actual hydrogen bonding scheme involving O24, O25, and O26 depends on their particular coordination by Ca, Na, or vacancies.

Relationships with other structures

The crystal structure of sailaufite is closely related to the structure type of mitridatite, $Ca_6(H_2O)_6[Fe^{3+}{}_9O_6(PO_4)_9]\cdot 3H_2O$ (Moore & Araki, 1977), i.e. $Ca_2Fe^{3+}{}_3O_2(PO_4)_3\cdot 3H_2O$, and its assumed analogues (Moore & Ito, 1974) robersite (Mn^{3+}-phosphate) and arseniosiderite (Fe^{3+}-arsenate). Close relationship also exists with the mineral pararobertsite, $Ca_2Mn^{3+}{}_3O_2(PO_4)_3\cdot 3H_2O$ (Roberts *et al.*, 1989), the structure of which was only recently solved by Kampf (2000). Table 6 compares their compositions, cell contents and lattice parameters with those of sailaufite.

In the mitridatite structure (Moore & Araki, 1977), the compact octahedral-tetrahedral sheet unit has the composition $[Fe^{3+}{}_9O_6(PO_4)_9]^{12-}$. In analogy to sailaufite, this sheet is built up from an isotypic arrangement of octahedral nonamer rings, whereas both, the AsO_4 tetrahedra and the CO_3 groups in sailaufite are replaced by PO_4 tetrahedra in mitridatite. Fig. 7a and 7b compare the resulting ring topologies. In spite of the spherical d^5 electron configuration of the Fe^{3+} cations, all $Fe^{3+}O_6$ octahedra exhibit much weaker, but completely analoguous bond length and angle distortions with four short and two longer Fe–O bonds, the latter located within the plane of the sheet according to Fig. 5. The corresponding overall mean <Fe–O> distances are 1.981 and 2.098 Å, respectively. Similar to sailaufite, the calcium-water layers are composed of $CaO_5(H_2O)_2$ polyhedra, condensed to dimers, and of isolated water molecules. According to Moore & Araki (1977), the apical oxygen atoms of those PO_4 tetrahedra replacing the CO_3 groups each only act as acceptors of two hydrogen bonds from water molecules bonded to Ca atoms. However, one of these apical O atoms obviously also contributes to the coordination of a Ca atom (Ca–O = 2.71 Å), thus resulting in an [8]-coordination for one of the six different Ca atoms. Compared to sailaufite, where the mirror plane of the calcium-water layers coincides with one mirror plane of the pseudo-trigonal (*P*31*m*) octahedral-tetrahedral sheets leading to space group *Cm*, the mirror plane of two consecutive calcium-water layers in mitridatite-type compounds is rotated by +120°, respectively –120° around the pseudotrigonal axes of the nonamer rings. This results in a violation of the mirror symmetry in mitridatite, a symmetry reduction to space group *Cc* with $c' \approx 2\times c$ (*Aa* setting in Moore & Araki, 1977), and a modification of the cell angle β. In principle, also a stacking with

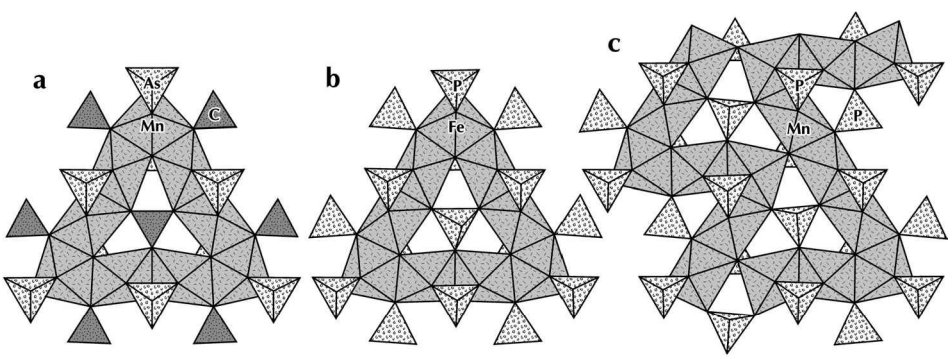

Fig. 7. Comparison of fundamental building blocks in sailaufite, mitridatite, and pararobertsite. a) octahedral nonamer ring with adjacent AsO_4 and CO_3 groups in sailaufite; b) octahedral nonamer ring with adjacent PO_4 groups in mitridatite; c) octahedral Z-shaped chains with adjacent PO_4 groups in pararobertsite.

Table 6. Comparison of sailaufite and structurally related minerals. The lattice parameters (Å, °) and space groups are transformed according to the setting of sailaufite.

name	idealized composition	SG	Z	*a*	*b*	*c*	β
sailaufite	$CaNaMn^{3+}{}_3O_2(AsO_4)_2(CO_3)\cdot 3H_2O$	*Cm*	6	11.25	19.63	8.93	100.1
mitridatite	$Ca_2Fe^{3+}{}_3O_2(PO_4)_3\cdot 3H_2O$	*Cc*	12	11.25	19.35	17.55	95.8
robertsite	$Ca_2Mn^{3+}{}_3O_2(PO_4)_3\cdot 3H_2O$	*Cc*	12	11.30	19.53	17.36	96.0
arseniosiderite	$Ca_2Fe^{3+}{}_3O_2(AsO_4)_3\cdot 3H_2O$	*Cc*	12	11.30	19.53	17.76	96.0
pararobertsite	$Ca_2Mn^{3+}{}_3O_2(PO_4)_3\cdot 3H_2O$	$P2_1/a$	4	11.06	13.23	8.81	101.2

three calcium-water layers – each one rotated by 120° – is possible, building a theoretical structure with trigonal symmetry and cell parameters $a \approx 11.3$ Å and $c'' \approx 3 \times c \approx 26.5$ Å. Besides, the frequent twinning and stacking faults observed in sailaufite samples are very probably related to these different possibilities of stacking calcium-water layers between the octahedral-tetrahedral layers in these structure types.

In pararobertsite (Kampf, 2000) the octahedral nonamer rings are broken and linked to edge sharing Z-shaped chains. These chains are interlinked by oxo-oxygens and PO_4 tetrahedra to a compact sheet of composition $[Mn^{3+}{}_6O_4(PO_4)_6]^{8-}$, *i.e.* equivalent to the Fe^{3+} bearing sheet in mitridatite. Fig. 7c compares the resulting assembly with the nonamer rings in sailaufite (Fig. 7a) and mitridatite (Fig. 7b). In contrast to the polar pseudotrigonal symmetries of the octahedral-tetrahedral rings in sailaufite and mitridatite, the Z-chain geometry in pararobertsite allows a centric arrangement of octahedra and tetrahedra, leading to space group $P2_1/c$ for pararobertsite with $b' \sim 2/3 \times b$. A remarkable feature in pararobertsite is the inversion of the Jahn-Teller distortion of one out of four different $Mn^{3+}O_6$ octahedra to a compressed pseudotetragonal dipyramid with two short and four longer Mn–O bonds. Like in sailaufite and mitridatite, the octahedral-tetrahedral sheets are connected via layers of dimer forming $CaO_5(H_2O)_2$ polyhedra and isolated water molecules.

Acknowledgements: The authors thank C.L. Lengauer, Vienna, for the measurement of the X-ray powder diffraction pattern, and T. Ntaflos, Vienna, for performing the EMP analyses. Useful comments by two reviewers, *i.e.* S. Merlino – especially on different layer stackings within this mineral group – and A. Kampf helped to improve the manuscript. M. A. gratefully acknowledges financial support by a research fellowship from the *Fonds zur Förderung der wissenschaftlichen Forschung*, Austria (project P13976-CHE). Further financial support by the *International Centre for Diffraction Data* (grant 90-03ET) is gratefully acknowledged.

References

Baur, W.H. (1981): Interatomic distance predictions for computer simulation of crystal structures. *in* "Structure and bonding in crystals, Vol. II", M. O'Keeffe & A. Navrotsky, eds. Academic Press, New York, 31-52.

Brugger, J., Krivovichev, S., Kolitsch, U., Meisser, N., Andrut, M., Ansermet, S., Burns, P. (2002): Description and crystal structure of manganlotharmeyerite, $Ca(Mn^{3+},\square,Mg)_2\{AsO_4,[AsO_2(OH)_2]\}_2(OH,H_2O)_2$, from the Starlera Mn-deposit, Swiss Alps, and a redefinition of lotharmeyerite. *Can. Mineral.*, **40**, 1597-1608.

Fischer, R.X. & Tillmanns, E. (1988): The equivalent isotropic displacement factor. *Acta Cryst. C*, **44**, 775-776.

Kampf, A.R. (2000): The crystal structure of pararobertsite and its relationship to mitridatite. *Am. Mineral.*, **85**, 1302-1306.

Libowitzky, E. (1999): Correlation of O–H stretching frequencies and O–H···O hydrogen bond lengths in minerals. *Monatsh. Chemie*, **130**, 1047-1059.

Lorenz, J. (1991): Die Mineralien im Rhyolithsteinbruch von Sailauf. *Aufschluss*, **42**, 1-38.

Moore, P.B. & Araki, T. (1977): Mitridatite, $Ca_6(H_2O)_6[Fe^{III}{}_9O_6(PO_4)_9]\cdot 3H_2O$. A noteworthy octahedral sheet structure. *Inorg. Chem.*, **16**, 1096-1106.

Moore, P.B. & Ito, J. (1974): Isotypy of robertsite, mitridatite, and arseniosiderite. *Am. Mineral.*, **59**, 48-59.

Nonius (1998): Kappa CCD program package. Nonius B.V., Delft.

Roberts, A.C., Sturman, B.D., Dunn, P.J., Roberts, W.L. (1989): Pararobertsite, $Ca_2Mn^{3+}{}_3(PO_4)_3O_2\cdot 3H_2O$, a new mineral species from the Tip Top pegmatite, Custer County, South Dakota, and its relationship to robersite. *Can. Mineral.*, **27**, 451-455.

Shannon, R.D. (1976): Revised effective ionic radii and systematic studies of interatomic distances in halides and chalcogenides. *Acta Cryst. A*, **32**, 751-767.

Sheldrick, G.M. (1997): SHELX-97, a program suite for crystal structure solution and refinement. Universität Göttingen.

Received 3 June 2002
Modified version received 21 November 2002
Accepted 16 January 2003